A facile method to enhance the performance of soil bioelectrochemical systems using *in situ* reduced graphene oxide

Claudia Camedda,[1,2] Robert D. Hoelzle,[3] Alessandra Carucci,[2] Stefano Milia,[4] and Bernardino Virdis[1,*]

[1] The University of Queensland, Advanced Water Management Centre, Gehrmann Building (60), Brisbane Qld 4072, Australia.

[2] University of Cagliari, Department of Civil-Environmental Engineering and Architecture (DICAAR), Via Marengo 2, 09123 Cagliari, Italy.

[3] The University of Queensland, Australian Centre for Ecogenomics, School of Chemistry and Molecular Biosciences, Brisbane Qld 4072, Australia.

[4] National Research Council of Italy, Institute of Environmental Geology and Geoengineering, Via Marengo 2, 09123 Cagliari, Italy.

* Correspondence to:
Dr Bernardino Virdis
The University of Queensland, Advanced Water Management Centre,
Level 4, Gehrmann Building (60), Brisbane Qld 4072, Australia
Telephone: +61 7 3365 4730
Fax: +61 7 3365 4726
Email: b.virdis@uq.edu.au

DOI: http://dx.doi.org/10.1016/j.electacta.2019.134881

Abstract

Bioelectrochemical systems offer a potential solution for the treatment of a broad variety of environmental contaminants. Unfortunately, when applied to the remediation of soil and sediments, the low electrical and hydraulic conductivities of these media limit their effective applicability in full-scale installations. Interestingly, these drawbacks may be overcome by including conductive particles within the soil porosity in order to maximize the outreach of the electrode through the contaminated medium, thereby minimizing electron- and mass-transfer limitations.

Herein, we increase the electrical conductivity of a model porous aquifer by using amendments of graphene oxide (GO), followed by its reduction into reduced graphene oxide (rGO) by means of microbial or electrochemical reduction methods. Both approaches promoted the formation of rGO-sand composites with superior electrical features compared to controls not amended with GO, with conductivity being positively correlated to the GO application rates, within the applied range of 10 to 2000 mg_{GO} kg_{sand}^{-1}. The electrochemical reduction yielded significantly higher conductivity than the biological method. This result is putatively ascribed to a higher degree of reduction achieved by the former approach. When applied to laboratory scale soil bioelectrochemical systems fed with sodium acetate as a model contaminant, the GO-amended reactors delivered 32x higher anodic current compared to unamended controls. We conclude that GO amendments to porous soils improve the outreach of the electrochemical process to include microbial cells in distal soil locations.

Keywords: microbial electrochemical technologies; bioremediation; reduced graphene oxide; electrode modification; improved soil conductivity.

1 Introduction

Groundwater and soil contamination by recalcitrant and hazardous organic compounds such as petroleum hydrocarbons derived from anthropogenic sources (*e.g.*, industrial development, intensive agriculture practices, and accidental oil spills), poses a serious worldwide concern. Besides expensive physico-chemical treatment technologies, bioremediation processes that rely on the microbially-mediated destruction of pollutants, are increasingly becoming the treatment of choice, even for the removal of more persistent and toxic pollutants, due to their cost-effectiveness and flexibility [1]. During bioremediation, microorganisms use organic contaminants as a source of energy and carbon to fulfil their metabolic requirements [2]. Since terminal electron acceptors such as oxygen and nitrates are typically present at low levels in natural subsurface environments [3,4], bioremediation technologies often rely on the continuous supply of these chemicals to promote microbial respiration and hence the degradation process [5]. Unfortunately, the presence of unwanted side reactions (*e.g.*, the reaction of oxygen with reduced species such as Fe^{2+} and Mn^{2+}), the limited dispersion of these chemicals in the soil matrix, and losses due to diffusion from the contaminated area, requires that these chemicals are supplied in large excess relatively to the stochiometric demand to treat the contamination [3,5], resulting in significant operational costs and energy investment [6].

Conversely, microbial electrochemical technologies, might provide a valid alternative to conventional processes for plume management [7]. By employing the specific ability of certain microorganisms to use solid state electrodes as electron acceptors or donors, bioelectrochemical systems (BESs) were applied to promote the removal of a wide range of groundwater and soil contaminants, including BTEX [6], PAHs [8], nitrates [9], and chlorinated aliphatic hydrocarbons [10]. Importantly, since electrodes in BESs act as an inexhaustible sink or source of electrons to sustain the microbial metabolism, bioelectrochemical remediation overcomes the requirement for expensive chemical dosing and might offer a cheaper alternative to conventional technologies for bioremediation [1,11].

While potentially competitive with other conventional treatments, the bioelectrochemical remediation of soil and groundwater contaminants is generally associated to low anodic currents, typically within the range of a few micro Amperes per square centimetres of projected electrode surface [8,12–14]. Factors affecting the

low performance include the usually slow biodegradability of certain contaminations (*e.g.*, BTEX and PAHs), as well as the intrinsic properties of the solid matrices. For example, in a standard configuration of a soil or sediment bioelectrochemical system, the electrodes are buried under the soil/water interface [15,16]. The presence of soil particles and the absence of hydraulic regimes to guarantee completely mixed conditions in the subsurface environment, usually generate strong concentration gradients around the electrodes, which limit the mass transport of contaminants towards the electrode surface [16,17]. In addition, since bioelectrocatalytic reactions are usually confined to the surface of the electrodes where electroactive organisms are preferentially located, the effectiveness of the bioelectrochemical treatment is typically limited to a few centimetres near the electrode surface [5].

Amending soils or sediments with biocompatible conductive particles such as granular graphite, biochar, fumed silica, ferric citrate, colloidal iron oxyhydroxide, in order to increase their electrical conductivity has been proposed as a potential solution to resolve this important drawback of bioelectrochemical remediation technologies [17–20]. It is hypothesized that the presence of conductive particles would allow the simultaneous decrease of mass transport limitations of contaminants towards the electrode surface, since the electrodes would stretch directly into the soil porosity through a network of conductive particles all electrically interconnected, while the increase in the electrode surface would promote the attachment of additional electroactive biomass that can contribute to the bioelectrochemical remediation, thereby achieving a significant improvement in performance of the bioelectrochemical treatment.

Along these lines is the use of graphene, a two-dimensional carbon nanomaterial characterized by outstanding electrical conductivity, high mechanical and chemical stability, and high specific surface area [21]. A cost-effective approach for graphene production is the reduction of water-soluble non-conductive graphene oxide (GO) to insoluble and conductive reduced graphene oxide (rGO). Amongst the various strategies for GO reduction, electrochemical reduction at polarized electrode surfaces, and microbial reduction by organisms that use GO as electron acceptor to support respiration, are the simplest and least expensive methods [22].

In this study, we tested the hypothesis that rGO significantly increases the electrical conductivity of porous soils by forming a network of conductive rGO particles extending several centimetres from the current collectors. We amended a

model porous soil (quartz sand) with different levels of GO and employed and compared two strategies for the *in situ* reduction of GO into rGO, specifically, biological GO reduction using electroactive microorganisms as biocatalysts and acetate as metabolic electron donor, and electrochemical GO reduction using polarized electrodes to induce the reduction. The use of dispersions of GO as opposed to direct graphene inclusions is advantageous. In fact, not only GO is cheaper than graphene, but the use of a water dispersion containing GO would also facilitate its inclusion within the soil porosity, thereby circumventing the need for mechanical mixing that would otherwise be necessary to incorporate previously prepared graphene nanoparticles.

Electrical conductivity of the rGO-sand composites was assessed as a function of the GO application rates using the two-probe DC current-Voltage (*i-V*) method. Measurements were confirmed with two-probe AC Impedance Spectroscopy. Raman spectroscopy was used to characterise the chemical nature of the aggregates formed upon the reduction process. 16S rRNA gene amplicon sequencing was employed to assess the microbial communities developed under different GO levels during the biological GO reduction tests. Finally, the performance of the GO amended soils was tested in bench-scale soil bioelectrochemical systems using acetate as a model organic contaminant.

2 Experimental

2.1 Aqueous mediums and model soil

Biological GO reduction tests were conducted in growth medium consisting of autoclaved reverse osmosis (RO) water containing, per litre: Na_2HPO_4 (6.0 g), KH_2PO_4 (3.0 g), NH_4Cl (0.1 g), NaCl (0.5 g), $MgSO_4 \cdot 7H_2O$ (0.1 g), $CaCl_2 \cdot 2H_2O$ (0.015 g), CH_3COONa (3.28 g, equivalent to 40 mmol), trace elements solution (1 mL, composition in Lu et al. [23]), and vitamin solution (1 mL, composition in Wolin et al. [24]). Electrochemical GO reduction tests were conducted in a medium consisting of RO water and 5.8 g L^{-1} NaCl, according to Hilder et al. [25]. Quartz sand (white quartz, 50-70 mesh, Sigma-Aldrich, USA) was used to simulate a porous soil.

2.2 Miniature-scale electrochemical systems

Tests of biological and electrochemical GO reduction were performed using ordinary polypropylene test tubes (internal volume 70 mL, Sarstedt AG & Co., Germany),

somewhat modified to accommodate two graphite rods (length: 7 cm, diameter: 6.35 mm, Morgan AM&T, Australia) placed at a fixed distance of *ca.* 2 cm. The rods were partially insulated with parafilm leaving only a portion about 1.2 cm long at the bottom (*i.e.*, the part buried in the sand) exposed to the electrolyte. A schematic representation of the miniature-scale electrochemical systems is provided in **Figures S1** and **S2** in the Supplementary Material.

In addition to the graphite rods, the test tubes used for the electrochemical GO reduction tests also contained a titanium wire (99.8 %, temper annealed, diameter 0.5 mm, 5 cm long, Advent Research Materials, UK) and an Ag/AgCl reference electrode in 3 M KCl (MF-2053, Basi, USA, +0.210 V *vs* the standard hydrogen electrode, SHE). Each test tube was partially filled with 30 g of sand, occupying *ca*. 20 mL of the volume of the tubes, and 30 mL of the respective electrolytes mixed with a GO dispersion (Graphene Oxide water dispersion, 4 g L^{-1}, Graphenea, Spain) in appropriate proportions to yield GO application rates of 10, 50, 100, 200, 500, 1000, and 2000 mg_{GO} kg_{sand}^{-1} (respectively 0.001, 0.005, 0.01, 0.02, 0.05, 0.1, 0.2 % of the dry weight of the sand). Additional tubes were prepared to contain only sand and the aqueous mediums, but without GO. These tubes were used as Controls as indicated in the text. pH and ionic conductivity of the electrolytes were measured prior to the reduction tests and are indicated in **Table S1** in the Supplementary Material.

2.3 Biological GO reduction

The biological GO reduction tests were done using the miniature-scale electrochemical systems design that only contained two graphite rods (**Figure S1**). The tests were carried out under the rationale that microorganisms use GO as electron acceptor during the metabolism of a carbonaceous electron donor (sodium acetate in this work), thereby forming rGO. Therefore, eight miniature-scale electrochemical systems (seven in total plus a control not amended with GO) were inoculated with 1 mL of electroactive biomass (**Text S1**). The tubes were sealed and incubated at 35° C for 14 d inside an anaerobic chamber to promote the conversion of GO into rGO. Preliminary tests performed in serum bottles had shown that this incubation time was sufficient to allow for the formation of solid particles (putatively made of rGO and bacterial cells) that clearly separated from the solution (**Text S2**). Measurements of conductivity of the rGO-sand composites were made at the start (0 d) and at the end (14 d) of the incubation period, according to the method described below.

2.4 Electrochemical GO reduction

The electrochemical GO reduction experiments were conducted using the set-up depicted in **Figure S2,** which, in addition to the two graphite rods, included a titanium wire and a reference electrode. After the addition of the respective mediums, the tubes were sealed and the electrodes connected to a multi-channel potentiostat to accommodate for the operation of all tubes simultaneously (1000C Series Multi-potentiostat, CH Instruments, Austin, Texas, USA). In each tube, the two graphite rods were short-circuited and connected to the working electrode terminal (WE), while the titanium wire was connected to the counter electrode terminal (CE). During the reduction, the WE was poised at the potential of -1.2 V *vs* Ag/AgCl for a total period of 60 h. This potential was considered sufficient to promote the progressive electrochemical reduction of GO into rGO [25]. Measurements of conductivity of the rGO-sand composites were performed prior to the start of the electrochemical reduction (0 h), and then at 12 h, 36 h and 60 h. Electrical conductivity was measured according to the methods described below.

2.5 Measurements of electrical conductivity

The conductivity of the rGO-sand composites obtained after the biological and electrochemical reduction was determined using the two-probe DC current-voltage (*i-V*) method, according to previously published procedure [26]. A fixed voltage was imposed between the two graphite rods using a potentiostat. While the WE terminal of the potentiostat was connected to one rod, the CE and REF terminals were short-circuited and connected to the second rod. This arrangement allowed the application of a fixed voltage bias between the CE/REF and the WE. The resulting anodic current was recorded over a 300 s period to allow for the exponential decay of ionic and capacitive charge/discharge currents. To guarantee linearity of the *i-V* features and avoid electrochemical splitting of water, discrete voltage values were selected within a low voltage ramp of ±0.5 V using 0.05 V increment/decrement steps (with the sole exception of the measurements made prior to the reduction, for which a narrower voltage ramp within ±0.3 V was used). For each voltage, time-averaged currents were determined using the data collected in the final 60 s, during which the steady-state was confirmed by a time-variation of the current below 20 μA min^{-1}. Time-averaged currents were used to create current *vs* voltage (*i-V*) profiles, which were fitted with a

linear function using Prism (Version 7.a, Graphpad, USA) to extract the slope (that is, the electrical conductance), whose inverse represents the electrical resistance, according to Ohm's law:

$$R_{i-V} = \frac{V}{i} \quad (1)$$

where $R_{i\text{-}V}$ is the electrical resistance as determined from the *i-V* profiles (Ω), V is the applied voltage (V) and i the steady-state current across the two rods (A). Values of resistance were then used to determine the electrical resistivity according to the following equation:

$$\rho = \frac{R \cdot A}{100 \cdot l} \quad (2)$$

where ρ is the electrical resistivity of the sample (Ω·m), R is the resistance (Ω), A is the projected sectional area of the rods (cm^2), l is the distance between the rods (cm). Finally, the electrical conductivity σ (mS cm^{-1}) was determined as the inverse of the resistivity:

$$\sigma = \frac{1}{\rho} \quad (3)$$

2.6 Confocal Raman Microscopy (CRM)

Confocal Raman Microscope measurements were performed at 22±1° C using an Alpha 300 Raman/AFM (WITec GmbH, Ulm, Germany) equipped with a frequency-doubled continuous-wave Nd:YAG laser to obtain a 532 nm excitation line. The laser beam was focused by an objective lens (Nikon 40X, N.A. 0.6, CFI S Plan Fluor ELWD objective). The back-scattered Raman light from the sample was collected with a 100 µm optical fibre employing a Raman spectrometer (1800 grooves per mm grating) with a charge-coupled device (EMCCD) spectroscopic detector. Project FOUR software (WITec GmbH, Ulm, Germany) was used for spectra processing and image reconstruction.

2.7 Bench-scale soil bioelectrochemical systems

Four bench-scale soil bioelectrochemical systems were assembled using tubular glass vessels (internal volume of *ca.* 450 mL), tailored to accommodate three graphite rods serving as working electrodes and current collectors (length: 12 cm, diameter: 6.35 mm, Morgan AM&T, Australia), one piece of reticulated vitreous carbon (RVC) foam (45 pores per inch, dimensions: 1 x 1 x 2 cm^3, Duocel, ERF Materials and Aerospace Corporation, USA) serving as counter electrode, and an Ag/AgCl reference electrode in 3 M KCl (MF-2053, Basi, USA). External contact of the RVC was obtained using a titanium wire. The three graphite rods were short-circuited and connected to the WE terminal of a multi-channel potentiostat (VMP3 Potentiostat/Galvanostat, BioLogic Science Instruments, France), while the RVC and the reference electrode were connected to the CE and REF terminals, respectively.

Two of the four vessels were filled with 250 g of sand (equal to a volume of approximately 190 mL), and 250 mL of electrolyte, which included 125 mL of saline medium containing 5.8 g L^{-1} of NaCl in RO water and 125 mL of GO dispersion to yield a GO rate of 2000 mg_{GO} kg_{sand}^{-1} in the vessels. All graphite rods were partially insulated to leave only a portion about 3 cm long exposed to the electrolyte (*i.e.*, the part buried into the sand bed). rGO formation was achieved using the electroreduction method, whereby the graphite rods were poised at the potential of -1.2 V *vs* Ag/AgCl for a total period of 70 h, considered sufficient to achieve full reduction of the GO provided. After the electroreduction, the saline medium was drained and replenished with culturing medium (composition provided above), which included 40 mM of sodium acetate. Mixing was provided by including a hydraulic loop to recirculate the medium through the sand bed at the rate of *ca*. 100 mL h^{-1} using a peristaltic pump (323S Watson-Marlow Pty Limited NSW, Australia). A glass bottle containing additional 500 mL of medium was connected to the recirculation loop to provide additional buffering capacity and metabolic electron donor. We refer to these two vessels as rGO 1 and rGO 2. The two additional vessels were set-up identically to rGO 1 and rGO 2, except that these two systems were not amended with GO, and served as controls. They are referred herein as C1 and C2.

All four electrochemical systems were immersed in a water bath set at the temperature of 35 °C, and each was inoculated with 2.5 mL of electroactive biomass (**Text S1**). In each vessel, the graphite rods were short-circuited and poised at the fixed potential of 0 V *vs* Ag/AgCl and incubated for 20 d. This electrochemical potential was shown as suitable for the development of anodic biofilms metabolising acetate [27,28].

The resulting current *vs* time profiles were used to evaluate the performance of the systems.

3 Results and Discussion

To promote the biological reduction of GO, an enriched *Geobacter* community was used under the hypothesis that this highly electroactive lineage would directly aid in the reduction process and then be available for mediating electron transfer in the transition to a bioelectrochemical system. However, community analysis (**Supplementary method S1**) showed that after incubation (14 d) in the growth media containing 40 mM acetate as metabolic electron donor, *Geobacter* became a minor lineage in the system, never exceeding 2.5 % final abundance (**Figure S4**). Instead, lineages of *Acidovorax*, *Pseudomonas*, and to a lesser extent *Geovibrio*, overtook *Geobacter* as the dominant microbial community members. *Castellaniella*, *Xylophilus*, *Wolinella*, and one unidentified lineage were also highly abundant in the higher concentrations of GO. This change between the inoculum and the incubations accounted for about half (50.1 %) of the variance in the overall community profile, while about half (24.9 %) of the remaining variance resulted from the change in incubation GO concentration (**Figure S5**). The lower GO application rates (0 to 500 $mg_{GO}\ kg_{sand}^{-1}$) are distinguished from the highest (1000 and 2000 $mg_{GO}\ kg_{sand}^{-1}$) by high final abundance of *Pseudomonas*, *Geovibrio*, and *Acidovorax* lineages, while the higher concentrations are distinguished by *Castellaniella*, *Ferribacterium*, *Wolinella*, *Xylophilus*, *Azospirillum*, and a different lineage of *Pseudomonas*. Species of *Acidovorax* are well-known to degrade aromatic compounds such as biphenyls [29–32] and phenanthrene [33]. Additionally, some lineages of *Acidovorax*, such as *A.* sp. Strain KKS102, are thought to be symbiotic with specific *Pseudomonas* lineages in aromatic-degrading mixed communities [34,35]. This aromatic degradation function is highly consistent with the reduction of GO to rGO, and the high degree of associated variance between *Acidovorax* and *Pseudomonas_1* suggests these two lineages may be symbionts in this process. *Castellaniella* is also known to degrade aromatic compounds [36]. Its low abundance at GO up to 500 $mg_{GO}\ kg_{sand}^{-1}$, and then subsequent high abundance suggests that *Acidovorax* was able to outcompete *Castellaniella* at these lower GO concentrations, but that above 500 $mg_{GO}\ kg_{sand}^{-1}$ GO was in excess for *Acidovorax*, enabling other aromatic degraders to contribute to GO reduction. These

results are in disagreement with the hypothesis that the presence of GO might promote the enrichment towards microbial taxa with known extracellular electron transfer capabilities, as previously suggested by Alonso et al. [37], but are in line with community analysis performed on rGO-biofilm hydrogels and reported by Virdis and Dennis [38].

Conversely, the electrochemical GO reduction was obtained under abiotic conditions by poising the two graphite rods at the electrochemical potential of -1.2 V *vs* Ag/AgCl for a period of 60 h. In fact, according to the approach suggested by Hilder et al. [25], the application of a potential lower than -1.153 V *vs* Ag/AgCl ensures the formation of stable rGO deposits if the ionic conductivity and the pH of the electrolyte, both measured prior to starting the reduction, are within the ranges of 4 to 25 mS cm^{-1}, and 1.5 to 12.5, respectively, conditions that were adequately satisfied in the electrolytes used in this work (**Table S1**). The application of a reducing potential at the electrode/GO dispersion interface results in chemical and structural changes of the graphene oxide due to the progressive removal of the oxygen functional groups (COH, C=O, or COOH) present in GO [25], with the remaining oxygen groups producing structural defects compared to pristine graphene. Importantly, while GO sheets present low electrical conductivity, the progressive reduction results in the partial recovery of the conductivity [39]. The structural changes resulting from the reduction of GO into rGO are typically reflected in the spectroscopic signatures. **Figure 1** shows confocal Raman microscopy measurements on samples collected after the reduction process. The Raman scattering of graphene typically exhibit two principle bands designed as the G and the 2D at around 1580 and 2700 cm^{-1}, respectively, while a third band (D-band) is often observable at around 1350 cm^{-1} and is associated with defects within the carbon [40]. All three bands are clearly visible in all spectra measured on the collected samples, including the GO solution as provided by the manufacturer (**Figure 1A**), the material collected from the biological reduction test tubes at the end of the reduction processes (14 d) (**Figure 1B**), and after electrochemical reduction (60 h) (**Figure 1C**). All spectra present a very pronounced D-band, indicating a high level of structural disorder, probably ascribed to a multi-layered structure typical of the formation conditions. The formation of rGO from the reduction of GO due to the operating conditions is confirmed by changes in the relative intensity of the G- and D-bands. In particular, the ratio of the intensities of these two bands (I_D/I_G) is typically higher in rGO than in GO due to the increase in structural defects (resulting in the increase in the intensity of the D-band)

and the disruption of the sp^2 bonds of the carbon in rGO (resulting in a decrease in the intensity of the G-band) [40,41]. **Figure 1** shows that upon reduction, spectra collected from the aggregates present I_D/I_G ratios higher than the value observed in the GO dispersion, indicating that both reduction methods resulted in the formation of new graphitic domains following the reduction or removal of oxygen-containing functional groups [42]. Interestingly, a higher I_D/I_G ratio was observed on samples obtained after electrochemical reduction, and points at a higher degree of reduction and electrical properties achieved with this reduction method compared to the biological reduction route [39,40,43].

Figure 2 presents representative current-voltage profiles obtained during the measurements of conductivity using the two-probe DC *i-V* method. For both the biological and the electrochemical reduction methods, the profiles display high current response at increasing levels of GO, consistent with an increase in conductivity ascribed to the inclusion of rGO connecting the two current collectors. The same linear trend was observed on forward and backward scans, confirming the presence of ohmic contact of the junction [26]. It is worth noting that while the presence of acetate in the biological GO reduction miniature-scale electrochemical systems could potentially affect the measurements of conductivity because of the current associated with microbial acetate oxidation, this possible issue was ruled out here since the contribution of acetate-driven current would have resulted in a non-linear dependency of the current-Voltage profiles, typically observed in microbially-mediated electrochemical processes, and not evidenced in the *i-V* traces reported here (**Figure 2**). Indeed, Malvankar et al. [26] have previously reported that biofilm conductivity (measured across a similar voltage ramp as that used here) was not affected by acetate removal, thereby supporting our simplification.

The slopes of the linear fitting lines of the *i-V* profiles were used to determine the conductivity according to the methods described in the Experimental (**section 2**). **Figure 3** and **Table S2** report the values of conductivity for the full set of experiments. The measurements of conductivity obtained with the DC *i-V* method are in good agreement with those obtained using the two-probe AC impedance spectroscopy method (**Supplementary method S2** and **Text S3**), thereby confirming that the measured conductivity with the two-probe DC *i-V* method was due to the properties of the junction and not to those of the electrolyte. Interestingly, the increment in soil conductivity is positively correlated with the levels of GO. Not surprisingly, the highest

conductivities were measured at the highest GO application rate of 2000 mg_{GO} kg_{sand}^{-1}. Specifically, as the result of the electrochemical reduction, the soil conductivity increased from 0.0023±0.0003 mS cm^{-1} measured in the unamended control, to 19.7±0.9 mS cm^{-1} measured after 60 h of reduction, which is equal to a four-order of magnitude increase (**Table S2**). Though not as remarkable as observed after the electrochemical reduction, the biological GO reduction also yielded a significant improvement in the electrical conductivity, which increased from 0.003±0.003 mS cm^{-1} measured in the unamended control, to 5.1±1.5 mS cm^{-1}. These conductivities are lower than those measured on rGO films obtained from GO reduction with various chemical reductants [44–46]. However, the different scales and geometries of the measuring apparatuses adopted here make it difficult to compare our results with measurements of sheet resistance of thin film with uniform thickness reported elsewhere. Nevertheless, the results reported here are remarkable when compared with the conductivity resulting from amendments with other conductive materials [17,47,48]. For example, Burrell et al. [48] reported electrical conductivity in the range of approximately 90 to 190 μS cm^{-1} measured in soils amended with 3 % (w/w) of biochar. Conversely, our results show that GO amendments to soil of only 0.2 % (w/w) are sufficient to yield a conductivity that is two orders of magnitude higher. This might represent a considerable advantage for the eventual scale up of the technology.

Remarkably, while the electrochemical reduction was applied for a total of 60 h, the largest increment in conductivity was achieved within the first 12 h of reduction. **Figure 3B** shows that the conductivity values at 12 h measured in the low GO application rates (0-500 mg_{GO} kg_{sand}^{-1}) were already very close to the highest values recorded at 60 h. Further reduction resulted only in a small increase. Surprisingly, at the highest GO application rates (that is, 1000 and 2000 mg_{GO} kg_{sand}^{-1}), the conductivities measured at 60 h were lower than those measured at 12 h and 36 h. We ascribe this phenomenon to the hydrogen evolution reaction - highly possible under the electrochemical conditions applied (-1.2 V *vs* Ag/AgCl) - which could have resulted in the formation of increasingly larger bubbles and the progressive displacement and hence the disruption of the conductive rGO network. Indeed, the accumulation of gas bubbles within the rGO-sand particles was evident throughout the reduction process.

The electrochemical GO reduction method yielded consistently higher conductivity than the biological approach, especially at the higher GO applications rates. The relationship between the conductivity obtained with the two methods is

reported in **Figure S7**. At the GO rate of 2000 mg_{GO} kg_{sand}^{-1}, the electrochemical GO reduction resulted in rGO-sand composites displaying 4.1±1.3 times higher conductivity than that observed in the biological test tubes. We ascribe the better performance of the electrochemical method to the superior conductive properties of the rGO produced by the electrochemical reduction. Raman measurements corroborate this hypothesis, evidencing that the electrochemical reduction yielded rGO with a higher degree of reduction than the rGO produced through the biological method, as evidenced by assessment of the I_D/I_G ratios (see **Figure 1** and discussion above). The higher degree of reduction should translate into a higher electrical conductivity of the rGO deposits. Indeed, Mohan and co-workers observed that I_D/I_G ratio correlates well with higher electrical conductivity exhibited by GO reduced by different chemical reductants [39]. While it is also possible that the lower performance of the rGO produced through biological reduction is due to uncomplete reduction of the GO made available during the tests, our preliminary assessment in serum flasks (**Text S2** and **Figure S3**) show that all the GO provided was converted into graphitic deposits even at the highest application rates, suggesting that the 14 d incubation period was sufficient to allow the reduction of all the GO supplied. In addition, electrochemical impedance spectroscopy measurements performed at the end of the biological reduction period evidenced consistent values of the electrolyte resistance, and hence similar electrical properties of the electrolytes, maintained across the whole range of GO loads (**Text S3**).

These results revealed the superiority of the electrochemical reduction strategy in increasing the electrical conductivity of the model porous soil, with the highest conductivity resulting at GO application rate of 2000 mg_{GO} kg_{sand}^{-1} (**Figures 2** and **3**). In order to evaluate the performance of the augmented soil in terms of its capacity to act as an inexhaustible sink for electrons during the oxidation of carbonaceous organic matter, two identical bench-scale soil BESs were amended with 2000 mg_{GO} kg_{sand}^{-1} electrochemically reduced to rGO, filled with biological growth medium including 40 mM of acetate as metabolic electron donor, and seeded with electroactive biomass (**Figure S11**). The choice to use acetate as the metabolic electron donor was dictated by the requirement to use a readily biodegradable carbonaceous electron donor that would allow the assessment of the performance of the system without the constraint given by the slow degradation kinetics typical of more relevant soil and sediments contaminations such as, for instance, polycyclic aromatic hydrocarbons [12,49–52]. **Figure 4A** displays the current *vs* time profiles resulting from the operation of the

451 microbial electrochemical systems for a total of 22 d, during which two additional
452 acetate injections were done. After an initial lag associated with the time required for
453 the growth and colonization of the electrode surface by the electroactive community,
454 both GO-amended BESs delivered anodic current outputs consistently higher than those
455 measured in the control BESs (**Figure 4A** and **B**). The average peak current values
456 measured in the presence of rGO were improved by a factor of 32±10 (**Figure 4C**).
457 Considering that the current in the control reactors presumably derives only from
458 microbial cells interacting directly with the current collectors (*i.e.*, at the surface of the
459 graphite rods), the enhanced current observed in the GO-amended systems can be
460 interpreted by including also the contribution of microbial cells dwelling in locations
461 distant from the graphite rods. In fact, given that the electrical conductivity measured
462 between the rods was of the same magnitude as that measured in the miniature-scale
463 electrochemical systems (data not shown), and that the average distance between the
464 rods inserted in each reactor was of 5.0±0.3 cm, while the diameter of the vessels was
465 of 9 cm, it is reasonable to assume that all soil locations in the GO amended systems
466 were electrically interconnected thanks to the presence of rGO particles, with the
467 electrochemical process extending several centimetres into the soil from the graphite
468 rods. The highest peak anodic current of 103 mA was observed in reactor rGO 2 during
469 the third batch test (**Figure 4A**). Under the assumption that all soil volume (*ca.* 190
470 mL) is actively contributing to the electrochemical process, due to the presence of
471 electroactive microorganisms attached to the rGO, this electrical current is equivalent
472 to 0.542 mA cm^{-3} rGO-sand composite. When normalized to the surface of the graphite
473 rods in direct contact with the rGO in the sand bed (equal to 18.9 cm^2), the resulting
474 current density is 5.4 mA cm^{-2}, which not only is greater than values previously reported
475 for sand, soils, and sediments BESs following amendments of granular graphite, silica
476 or iron colloids, and biochar as conductive particles [17,18,20,53], thus indicating the
477 effectiveness of GO in enhancing the conductivity of porous soils, but being also higher
478 than current densities typically reported for anodic electroactive microorganisms
479 (including the highly performing *G. sulfurreducens* strain KN400), it implies that the
480 presence of rGO allows a larger portion of soil microbiome to contribute to the
481 electrochemical process [27,54,55].

4 Conclusions

In this study, a novel approach for the improvement of the electrochemical performance of soil bioelectrochemical systems is presented, based on the addition of GO into a porous soil, followed by its *in situ* reduction into rGO by means of electrochemical or microbial reduction methods. Measurements of conductivity by two-probe DC and AC methods indicated that the electrochemical reduction yielded rGO-sand composites with superior electrical conductivity than the biological approach. The presence of conductive rGO allows a larger soil volume (including the microbial community within) to contribute to the electrochemical process, thereby improving the outreach of the electrochemical treatment to include distal soil locations from the main current collectors. GO appears as more effective than other previously tested conductive materials in improving the performance of soil BESs, such as granular graphite, biochar, fumed silica, or a combination of ferric citrate and colloidal iron oxyhydroxide [17–20]. In the present study, it was observed that an improvement in the anodic current by an average factor of 32 relatively to unamended controls could be achieved using only a 0.2 % GO amendment to sand, equivalent to 2 kg GO per ton of soil (dry wt.), which is a significantly lower application rate than those used in the above-mentioned studies. With market projections for graphene expected to significantly expand over the next five to ten years, it is anticipated that the price of GO will drop significantly in the near future [56]. This is likely to promote the application of GO into next generation electrochemical waste treatment processes, including water and soil remediation, in line with current trends (see *e.g.*, Wang et al. [57], Colunga et al. [58], Shen et al. [59]). Moreover, various reports already exist on the sustainable production of graphene and graphene oxide from a variety of natural and industrial waste [60–62]. This may generate further incentives to promote the use of sustainably-sourced graphenes within the circular economy. In this scenario, provided that target electric currents (hence, conversion rates of contaminants) are met, GO-augmented soil bioelectrochemical systems might inspire the development of robust, flexible, low-cost, and sustainable alternative to traditional technologies for groundwater and soil remediation.

Acknowledgements

This research was funded by the Australian Research Council (ARC) through Discovery Project DP160102308. BV acknowledges the support of the ARC through

514 Australian Laureate Fellowship FL170100086. CC was supported by the University of
515 Cagliari, Italy, through the PhD program in 'Earth and Environmental Sciences and
516 Technologies'. Confocal Raman spectroscopy was performed at the Queensland node
517 of the Australian National Fabrication Facility, a company established under the
518 National Collaborative Research Infrastructure Strategy to provide nano- and micro-
519 fabrication facilities for Australia's researchers. Dr Bogdan Donose is acknowledged
520 for the support provided on the Raman spectroscopy measurements.
521

522 **References**

523 [1] M. Majone, R. Verdini, F. Aulenta, S. Rossetti, V. Tandoi, N. Kalogerakis, S.
524 Agathos, S. Puig, G. Zanaroli, F. Fava, In situ groundwater and sediment
525 bioremediation: Barriers and perspectives at European contaminated sites, N.
526 Biotechnol. 32 (2015) 133–146. doi:10.1016/j.nbt.2014.02.011.

527 [2] P. Alvarez, W. Illman, Bioremediation and Natural Attenuation, 2006.
528 doi:10.1007/s13398-014-0173-7.2.

529 [3] M. Kronenberg, E. Trably, N. Bernet, D. Patureau, Biodegradation of polycyclic
530 aromatic hydrocarbons: Using microbial bioelectrochemical systems to
531 overcome an impasse, Environ. Pollut. 231 (2017) 509–523.
532 doi:10.1016/j.envpol.2017.08.048.

533 [4] K. Rabaey, Bioelectrochemical Systems: From Extracellular Electron Transfer
534 to Biotechnological Application, 2009. doi:10.2166/9781780401621.

535 [5] M. Daghio, F. Aulenta, E. Vaiopoulou, A. Franzetti, J.B.A. Arends, A. Sherry,
536 A. Suàrez-Suàrez, I.M. Head, G. Bestetti, K. Rabaey, Electrobioremediation of
537 oil spills, Water Res. 114 (2017) 351–370. doi:10.1016/j.watres.2017.02.030.

538 [6] T. Zhang, S.M. Gannon, K.P. Nevin, A.E. Franks, D.R. Lovley, Stimulating the
539 anaerobic degradation of aromatic hydrocarbons in contaminated sediments by
540 providing an electrode as the electron acceptor, Environ. Microbiol. 12 (2010)
541 1011–1020. doi:10.1111/j.1462-2920.2009.02145.x.

542 [7] O. Modin, F. Aulenta, Three promising applications of microbial
543 electrochemistry for the water sector, Environ. Sci. Water Res. Technol. 3 (2017)
544 391–402.

545 [8] L. Lu, H. Yazdi, S. Jin, Y. Zuo, P.H. Fallgren, Z.J. Ren, Enhanced
546 bioremediation of hydrocarbon-contaminated soil using pilot-scale
547 bioelectrochemical systems, J. Hazard. Mater. 274 (2014) 8–15.
548 doi:10.1016/j.jhazmat.2014.03.060.

549 [9] B. Virdis, K. Rabaey, Z. Yuan, R.A. Rozendal, J. Keller, Electron Fluxes in a
550 Microbial Fuel Cells Performing Carbon and Nitrogen Removal.pdf, Environ.
551 Sci. Technol. 43 (2009) 5144–5149.

552 [10] F. Aulenta, A. Canosa, P. Reale, S. Rossetti, S. Panero, M. Majone, Microbial

reductive dechlorination of trichloroethene to ethene with electrodes serving as electron donors without the external addition of redox mediators, Biotechnol. Bioeng. 103 (2009) 85–91. doi:10.1002/bit.22234.

[11] H. Wang, H. Luo, P.H. Fallgren, S. Jin, Z.J. Ren, Bioelectrochemical system platform for sustainable environmental remediation and energy generation, Biotechnol. Adv. 33 (2015) 317–334. doi:10.1016/j.biotechadv.2015.04.003.

[12] M. Sherafatmand, H.Y. Ng, Using sediment microbial fuel cells (SMFCs) for bioremediation of polycyclic aromatic hydrocarbons (PAHs), Bioresour. Technol. 195 (2015) 122–132. doi:10.1016/j.biortech.2015.06.002.

[13] X. Li, X. Wang, Y. Zhang, Q. Zhao, B. Yu, Y. Li, Q. Zhou, Salinity and Conductivity Amendment of Soil Enhanced the Bioelectrochemical Degradation of Petroleum Hydrocarbons, Sci. Rep. 6 (2016) 1–11. doi:10.1038/srep32861.

[14] X. Li, X. Wang, Q. Zhao, L. Wan, Y. Li, Q. Zhou, Carbon fiber enhanced bioelectricity generation in soil microbial fuel cells, Biosens. Bioelectron. 85 (2016) 135–141. doi:10.1016/j.bios.2016.05.001.

[15] C.E. Reimers, L.M. Tender, S. Fertig, W. Wang, Harvesting energy from the marine sediment - Water interface, Environ. Sci. Technol. 35 (2001) 192–195. doi:10.1021/es001223s.

[16] L.M. Tender, C.E. Reimers, H.A. Stecher, D.E. Holmes, D.R. Bond, D.A. Lowy, K. Pilobello, S.J. Fertig, D.R. Lovley, Harnessing microbially generated power on the seafloor, Nat. Biotechnol. 20 (2002) 821–825. doi:10.1038/nbt716.

[17] S. Chen, J. Tang, L. Fu, Y. Yuan, S. Zhou, Biochar improves sediment microbial fuel cell performance in low conductivity freshwater sediment, J. Soils Sediments. 16 (2016) 2326–2334.

[18] J.B.A. Arends, E. Blondeel, S.R. Tennison, N. Boon, W. Verstraete, Suitability of granular carbon as an anode material for sediment microbial fuel cells, J. Soils Sediments. 12 (2012) 1197–1206.

[19] A. Domínguez-Garay, A. Berná, I. Ortiz-Bernad, A. Esteve-Núñez, Silica colloid formation enhances performance of sediment microbial fuel cells in a low conductivity soil, Environ. Sci. Technol. 47 (2013) 2117–2122. doi:10.1021/es303436x.

[20] Y.-L. Zhou, Y. Yang, M. Chen, Z.-W. Zhao, H.-L. Jiang, To improve the performance of sediment microbial fuel cell through amending colloidal iron oxyhydroxide into freshwater sediments, Bioresour. Technol. 159 (2014) 232–239.

[21] K.S. Novoselov, A.K. Geim, S. V. Morozov, D. Jiang, Y. Zhang, S. V. Dubonos, I. V. Grigorieva, A.A. Firsov, Electric field in atomically thin carbon films, Science (80-.). 306 (2004) 666–669. doi:10.1126/science.1102896.

[22] C.K. Chua, M. Pumera, Chemical reduction of graphene oxide: a synthetic chemistry viewpoint, Chem. Soc. Rev. 43 (2014) 291–312.

[23] H. Lu, A. Oehmen, B. Virdis, J. Keller, Z. Yuan, Obtaining highly enriched cultures of Candidatus Accumulibacter phosphates through alternating carbon sources, Water Res. 40 (2006) 3838–3848.

[24] E.A. Wolin, M. Wolin, R.S. Wolfe, Formation of methane by bacterial extracts,

597 J. Biol. Chem. 238 (1963) 2882–2886.

598 [25] M. Hilder, B. Winther-Jensen, D. Li, M. Forsyth, D.R. MacFarlane, Direct
599 electro-deposition of graphene from aqueous suspensions, Phys. Chem. Chem.
600 Phys. 13 (2011) 9187–9193. doi:10.1039/c1cp20173e.

601 [26] N.S. Malvankar, M. Vargas, K.P. Nevin, A.E. Franks, C. Leang, B.-C. Kim, K.
602 Inoue, T. Mester, S.F. Covalla, J.P. Johnson, V.M. Rotello, M.T. Tuominen,
603 D.R. Lovley, Tunable metallic-like conductivity in microbial nanowire
604 networks, Nat. Nanotechnol. 6 (2011) 573–579. doi:10.1038/nnano.2011.119.

605 [27] B. Virdis, D. Millo, B.C. Donose, D.J. Batstone, Real-time measurements of the
606 redox states of c-type cytochromes in electroactive biofilms: A confocal
607 resonance raman microscopy study, PLoS One. 9 (2014).
608 doi:10.1371/journal.pone.0089918.

609 [28] B. Virdis, D. Millo, B.C. Donose, Y. Lu, D.J. Batstone, J.O. Krömer, Analysis
610 of electron transfer dynamics in mixed community electroactive microbial
611 biofilms, RSC Adv. 6 (2016) 3650–3660. doi:10.1039/c5ra15676a.

612 [29] Y. Ohtsubo, F. Maruyama, H. Mitsui, Y. Nagata, M. Tsuda, Complete genome
613 sequence of Acidovorax sp. strain KKS102, a polychlorinated-biphenyl
614 degrader, (2012).

615 [30] M. Fukuda, Y. Yasukochi, Y. Kikuchi, Y. Nagata, K. Kimbara, H. Horiuchi, M.
616 Takagi, K. Yano, Identification of the bphA and bphB genes of Pseudomonas
617 sp. strain KKS102 involved in degradation of biphenyl and polychlorinated
618 biphenyls, Biochem. Biophys. Res. Commun. 202 (1994) 850–856.

619 [31] Y. Kikuchi, Y. Nagata, M. Hinata, K. Kimbara, M. Fukuda, K. Yano, M. Takagi,
620 Identification of the bphA4 gene encoding ferredoxin reductase involved in
621 biphenyl and polychlorinated biphenyl degradation in Pseudomonas sp. strain
622 KKS102., J. Bacteriol. 176 (1994) 1689–1694.

623 [32] K. Kimbara, T. Hashimoto, M. Fukuda, T. Koana, M. Takagi, M. Oishi, K. Yano,
624 Cloning and sequencing of two tandem genes involved in degradation of 2, 3-
625 dihydroxybiphenyl to benzoic acid in the polychlorinated biphenyl-degrading
626 soil bacterium Pseudomonas sp. strain KKS102., J. Bacteriol. 171 (1989) 2740–
627 2747.

628 [33] D.R. Singleton, J. Lee, A.N. Dickey, A. Stroud, E.H. Scholl, F.A. Wright, M.D.
629 Aitken, Polyphasic characterization of four soil-derived phenanthrene-degrading
630 Acidovorax strains and proposal of Acidovorax carolinensis sp. nov., Syst. Appl.
631 Microbiol. 41 (2018) 460–472.

632 [34] Y. Kikuchi, Y. Nagata, Y. Ohtsubo, T. Koana, M. Takagi, Pseudomonas
633 fluorescens KKL101, a benzoic acid degrader in a mixed culture that degrades
634 biphenyl and polychlorinated biphenyls, Biosci. Biotechnol. Biochem. 59 (1995)
635 2303–2304.

636 [35] K. Kimbara, T. Hashimoto, M. Fukuda, T. Koana, M. Takagi, M. Oishi, K. Yano,
637 Isolation and characterization of a mixed culture that degrades polychlorinated
638 biphenyls, Agric. Biol. Chem. 52 (1988) 2885–2891.

639 [36] P. Kämpfer, K. Denger, A.M. Cook, S.-T. Lee, U. Jäckel, E.B.M. Denner, H.-J.
640 Busse, Castellaniella gen. nov., to accommodate the phylogenetic lineage of
641 Alcaligenes defragrans, and proposal of Castellaniella defragrans gen. nov.,

642 comb. nov. and Castellaniella denitrificans sp. nov., Int. J. Syst. Evol. Microbiol.
643 56 (2006) 815–819.

644 [37] R.M. Alonso, M.I. San-Martín, A. Sotres, A. Escapa, Graphene oxide
645 electrodeposited electrode enhances start-up and selective enrichment of
646 exoelectrogens in bioelectrochemical systems, Sci. Rep. 7 (2017) 13726.

647 [38] B. Virdis, P.G. Dennis, The nanostructure of microbially-reduced graphene
648 oxide fosters thick and highly-performing electrochemically-active biofilms, J.
649 Power Sources. 356 (2017) 556–565. doi:10.1016/j.jpowsour.2017.02.086.

650 [39] V.B. Mohan, R. Brown, K. Jayaraman, D. Bhattacharyya, Characterisation of
651 reduced graphene oxide: Effects of reduction variables on electrical
652 conductivity, Mater. Sci. Eng. B. 193 (2015) 49–60.
653 doi:10.1016/J.MSEB.2014.11.002.

654 [40] L.G. Cançado, A. Jorio, E.H.M. Ferreira, F. Stavale, C.A. Achete, R.B. Capaz,
655 M.V.O. Moutinho, A. Lombardo, T.S. Kulmala, A.C. Ferrari, Quantifying
656 defects in graphene via Raman spectroscopy at different excitation energies,
657 Nano Lett. 11 (2011) 3190–3196.

658 [41] I.K. Moon, J. Lee, R.S. Ruoff, H. Lee, Reduced graphene oxide by chemical
659 graphitization, Nat. Commun. 1 (2010) 1–6. doi:10.1038/ncomms1067.

660 [42] S. Stankovich, D.A. Dikin, R.D. Piner, K.A. Kohlhaas, A. Kleinhammes, Y. Jia,
661 Y. Wu, S.B.T. Nguyen, R.S. Ruoff, Synthesis of graphene-based nanosheets via
662 chemical reduction of exfoliated graphite oxide, Carbon N. Y. 45 (2007) 1558–
663 1565. doi:10.1016/j.carbon.2007.02.034.

664 [43] S. Eigler, C. Dotzer, A. Hirsch, Visualization of defect densities in reduced
665 graphene oxide, Carbon N. Y. 50 (2012) 3666–3673.
666 doi:10.1016/j.carbon.2012.03.039.

667 [44] S. Pei, J. Zhao, J. Du, W. Ren, H.-M. Cheng, Direct reduction of graphene oxide
668 films into highly conductive and flexible graphene films by hydrohalic acids,
669 Carbon N. Y. 48 (2010) 4466–4474. doi:10.1016/J.CARBON.2010.08.006.

670 [45] J. Zhang, H. Yang, G. Shen, P. Cheng, J. Zhang, S. Guo, Reduction of graphene
671 oxide vial-ascorbic acid, Chem. Commun. 46 (2010) 1112–1114.
672 doi:10.1039/b917705a.

673 [46] S. Park, R.S. Ruoff, Chemical methods for the production of graphenes, Nat.
674 Nanotechnol. 4 (2009) 217. https://doi.org/10.1038/nnano.2009.58.

675 [47] L. Yu, Y. Yuan, J. Tang, Y. Wang, S. Zhou, Biochar as an electron shuttle for
676 reductive dechlorination of pentachlorophenol by Geobacter sulfurreducens, Sci.
677 Rep. 5 (2015). doi:10.1038/srep16221.

678 [48] L.D. Burrell, F. Zehetner, N. Rampazzo, B. Wimmer, G. Soja, Long-term effects
679 of biochar on soil physical properties, Geoderma. 282 (2016) 96–102.
680 doi:10.1016/J.GEODERMA.2016.07.019.

681 [49] J.M. Morris, S. Jin, Enhanced biodegradation of hydrocarbon-contaminated
682 sediments using microbial fuel cells, J. Hazard. Mater. 213–214 (2012) 474–477.
683 doi:10.1016/j.jhazmat.2012.02.029.

684 [50] Y. Zhang, X. Wang, X. Li, L. Cheng, L. Wan, Q. Zhou, Horizontal arrangement
685 of anodes of microbial fuel cells enhances remediation of petroleum

686 hydrocarbon-contaminated soil, Environ. Sci. Pollut. Res. 22 (2015) 2335–2341.
687 doi:10.1007/s11356-014-3539-7.

688 [51] X. Wang, Z. Cai, Q. Zhou, Z. Zhang, C. Chen, Bioelectrochemical stimulation
689 of petroleum hydrocarbon degradation in saline soil using U-tube microbial fuel
690 cells, Biotechnol. Bioeng. 109 (2012) 426–433. doi:10.1002/bit.23351.

691 [52] Z. Yan, N. Song, H. Cai, J.H. Tay, H. Jiang, Enhanced degradation of
692 phenanthrene and pyrene in freshwater sediments by combined employment of
693 sediment microbial fuel cell and amorphous ferric hydroxide, J. Hazard. Mater.
694 199–200 (2012) 217–225. doi:10.1016/j.jhazmat.2011.10.087.

695 [53] Y. Goto, N. Yoshida, Y. Umeyama, T. Yamada, R. Tero, A. Hiraishi,
696 Enhancement of Electricity Production by Graphene Oxide in Soil Microbial
697 Fuel Cells and Plant Microbial Fuel Cells, Front. Bioeng. Biotechnol. 3 (2015)
698 1–8. doi:10.3389/fbioe.2015.00042.

699 [54] K. Fricke, F. Harnisch, U. Schröder, On the use of cyclic voltammetry for the
700 study of anodic electron transfer in microbial fuel cells, Energy Environ. Sci. 1
701 (2008) 144–147. doi:10.1039/b802363h.

702 [55] H. Yi, K.P. Nevin, B.-C. Kim, A.E. Franks, A. Klimes, L.M. Tender, D.R.
703 Lovley, Selection of a variant of Geobacter sulfurreducens with enhanced
704 capacity for current production in microbial fuel cells, Biosens. Bioelectron. 24
705 (2009) 3498–3503.

706 [56] A. Zurutuza, C. Marinelli, Challenges and opportunities in graphene
707 commercialization, Nat. Nanotechnol. 9 (2014) 730.
708 https://doi.org/10.1038/nnano.2014.225.

709 [57] J. Wang, D. Wang, G. Liu, R. Jin, H. Lu, Enhanced nitrobenzene
710 biotransformation by graphene-anaerobic sludge composite, J. Chem. Technol.
711 Biotechnol. 89 (2014) 750–755. doi:10.1002/jctb.4182.

712 [58] A. Colunga, J.R. Rangel-Mendez, L.B. Celis, F.J. Cervantes, Graphene oxide as
713 electron shuttle for increased redox conversion of contaminants under
714 methanogenic and sulfate-reducing conditions, Bioresour. Technol. 175 (2015)
715 309–314. doi:10.1016/J.BIORTECH.2014.10.101.

716 [59] L. Shen, Z. Jin, D. Wang, Y. Wang, Y. Lu, Enhance wastewater biological
717 treatment through the bacteria induced graphene oxide hydrogel, Chemosphere.
718 190 (2018) 201–210. doi:10.1016/J.CHEMOSPHERE.2017.09.105.

719 [60] T. Somanathan, K. Prasad, K. Ostrikov, A. Saravanan, V. Krishna, Graphene
720 Oxide Synthesis from Agro Waste, Nanomaterials. 5 (2015) 826–834.
721 doi:10.3390/nano5020826.

722 [61] O. Akhavan, K. Bijanzad, A. Mirsepah, Synthesis of graphene from natural and
723 industrial carbonaceous wastes, RSC Adv. 4 (2014) 20441–20448.
724 doi:10.1039/c4ra01550a.

725 [62] K.H. Adolfsson, S. Hassanzadeh, M. Hakkarainen, Valorization of cellulose and
726 waste paper to graphene oxide quantum dots, RSC Adv. 5 (2015) 26550–26558.
727 doi:10.1039/c5ra01805f.

728

729

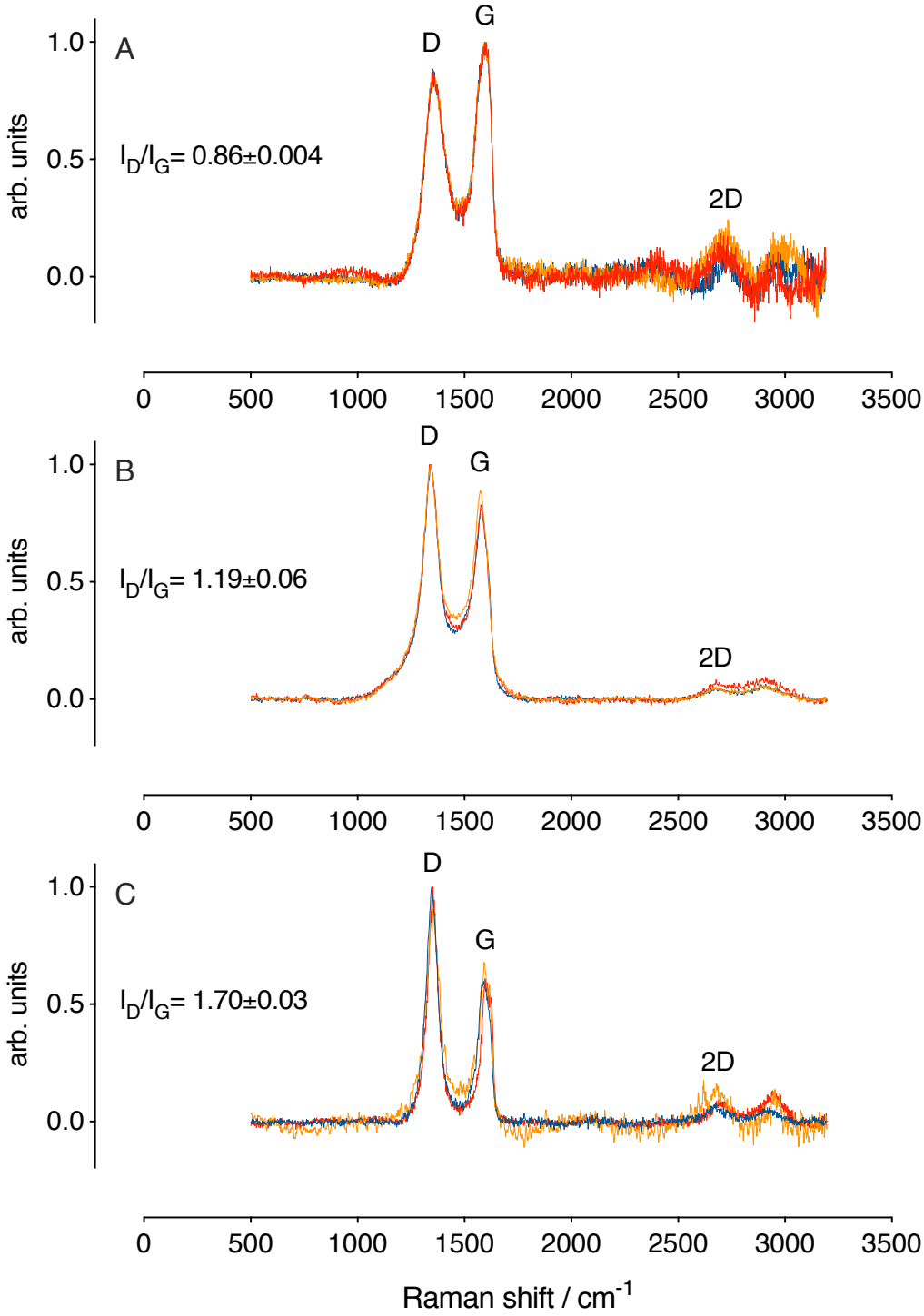

730

731 **Figure 1.** Normalized and background subtracted Raman spectra. (A) spectra of the
732 undiluted GO dispersion, (B) spectra of the graphitic material collected at the end of
733 the incubation period for the biological reduction (14 d), and (C) spectra of the graphitic
734 material collected at the end of the electrochemical reduction (60 h).

735

736

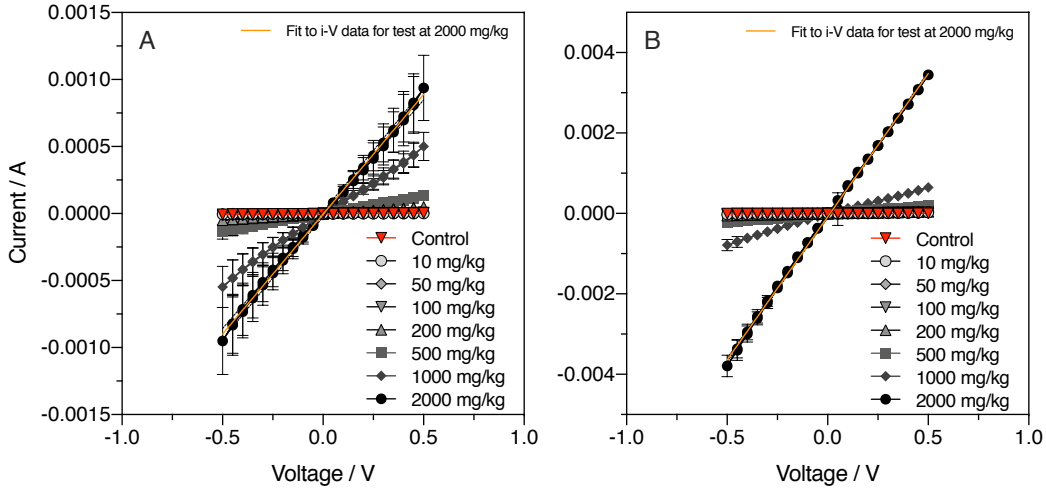

737

738 **Figure 2.** Representative current-voltage (*i-V*) data measured on rGO-sand composites
739 at the end of the respective reduction periods (*i.e.*, at 14 d for the biological GO
740 reduction, left panel, and at 60 h for the electrochemical reduction, right panel). Each
741 voltage was applied for 300 s across a voltage ramp of ±0.5 V using steps of 0.05 V.
742 Time-average currents were collected in the last 60 s and used to construct the *i-V*
743 profiles. Each data set was fit with a linear fitting function to determine the resistivity.
744 Data are reported as average and standard deviation of triplicate independent tests.
745 Individual tests are reported in **Figure S6**.

746

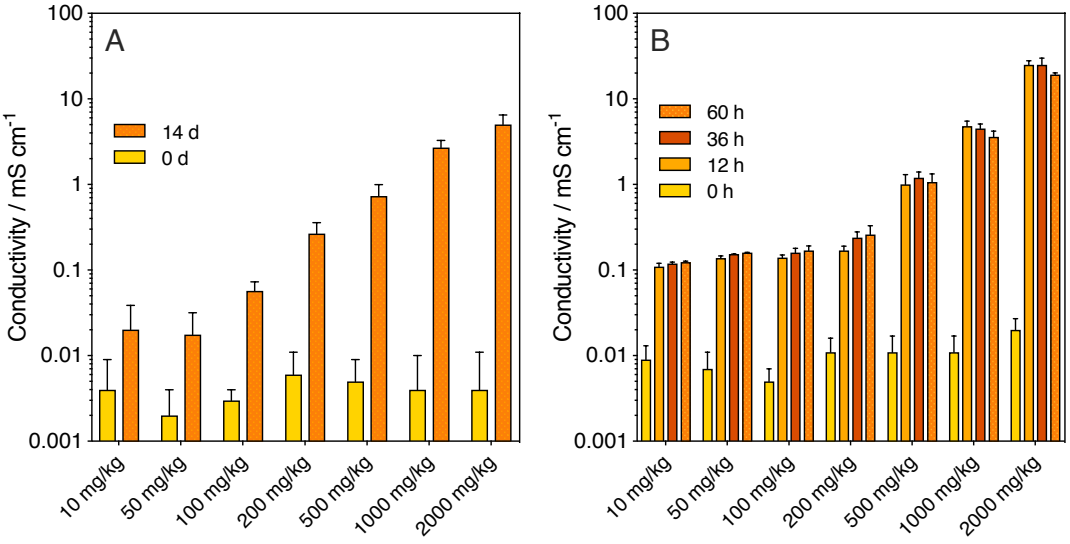

747

748 **Figure 3.** Electrical conductivity measured for different GO application rates (A) at
749 time 0 d and 14 d of incubation for the biological reduction, and (B) at time 0, 12, 36,
750 and 60 h of the electrochemical reduction.

751

752

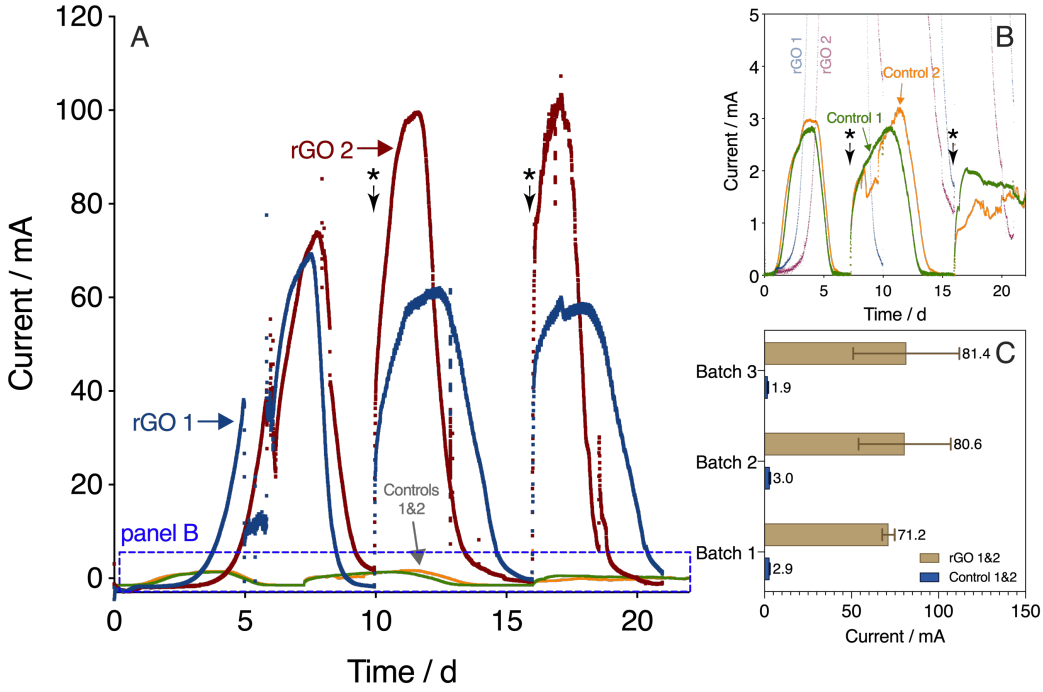

753

754 **Figure 4.** A) and B) electrical current *vs* time traces of soil bioelectrochemical systems
755 amended with GO at the rate of 2000 mg_{GO} kg_{sand}^{-1} (rGO 1 and rGO 2), and controls
756 unamended with GO (Control 1 and Control 2). 40 mM sodium acetate was provided
757 as metabolic electron donor. All electrochemical systems were seeded with
758 electroactive microorganisms. The electrodes were poised at 0 V *vs* Ag/AgCl for the
759 whole duration of the experiments. Asterisks represent acetate additions. C) average
760 current outputs produced during the course of the three batch tests.

761